





RESEARCH ARTICLE | SEPTEMBER 27 2023

## Photonic crystal textiles for heat insulation

Zebih Çetin   ; Yiğit Tunçtürk  ; H. Sami Sözüer 



*J. Appl. Phys.* 134, 123108 (2023)

<https://doi.org/10.1063/5.0157736>



View  
Online



Export  
Citation

CrossMark



**APL Quantum**  
Bridging fundamental quantum research with technological applications

**Now Open for Submissions**  
No Article Processing Charges (APCs) through 2024

**Submit Today**



# Photonic crystal textiles for heat insulation



Cite as: J. Appl. Phys. 134, 123108 (2023); doi: 10.1063/5.0157736

Submitted: 10 May 2023 · Accepted: 4 September 2023 ·

Published Online: 27 September 2023



Zebih Çetin,<sup>a)</sup> Yiğit Tunçtürk,<sup>b)</sup> and H. Sami Sözüer<sup>c)</sup>

## AFFILIATIONS

Physics Department, İzmir Institute of Technology, Gülbahçe Mah. Urla İzmir 35433, Türkiye

<sup>a)</sup>Author to whom correspondence should be addressed: zebihcetin@gmail.com

<sup>b)</sup>Electronic mail: ytnctrk@gmail.com

<sup>c)</sup>Electronic mail: samisozuer@iyte.edu.tr

## ABSTRACT

In this work, we have studied transmission properties of a photonic crystal-like structure that can be woven into fabrics. An interesting possibility emerges when considering the potential energy savings through suppression of radiation. It is a well-established fact that every object at a finite temperature inherently emits electromagnetic waves. Within the specific context of the human body, radiation takes on a crucial role as a fundamental mechanism governing heat dissipation. Thus, exploring ways to manage or mitigate this radiation could offer innovative approaches to optimize energy consumption and enhance heat regulation. It is well known that a photonic crystal can block electromagnetic energy with a specific frequency that is falling into a photonic bandgap. By using the numerical method called a finite-difference time domain, we have shown that this property of a periodic structure can be used to make textiles to save energy that is used to heat a human body environment. Numerical calculations have shown that by using the proposed photonic crystal structure, 53% of electromagnetic energy is reflected. Although we mainly focused on textiles, it is worth highlighting that the same fundamental principle can be extended to diverse fields; for example, this structure can be integrated with construction materials and effectively function as a radiation heat insulator.

Published under an exclusive license by AIP Publishing. <https://doi.org/10.1063/5.0157736>

## I. INTRODUCTION

Heat loss of the human body basically occurs in three different ways: convection and conduction, evaporation of moisture, and radiation.<sup>1–5</sup> Depending on the environmental conditions, such as wind, ambient temperature, relative humidity in the air, and the person's clothing, variations occur in the distribution of heat loss for these three different channels; for example, convection becomes the most important heat loss channel in windy weather. For someone lying on cold snow, heat loss by physical contact may be more important. However, under normal conditions, about two-thirds of the heat loss from the human body are through radiation.<sup>6</sup>

The intensity of the electromagnetic waves emitted by an ideal blackbody at temperature  $T$ , depending on the frequency, that is, the energy emitted from the unit area of the blackbody in unit time, in a unit frequency range, is given by Planck distribution,<sup>7</sup>  $u(\nu, T) = (8\pi h/c^3)\nu^3/(e^{h\nu/kT} - 1)$ , where  $h$  is Planck's constant,  $c$  is the speed of light,  $k$  is Boltzmann's constant, and  $\nu$  is the frequency. Integrating over the frequency and multiplying by the area of the object gives the energy emitted from the object per unit time,  $P_{emitted} = \epsilon A\sigma T^4$ , where  $A$  is the surface area of the object,  $\sigma$  is the Stephan-Boltzmann constant, and  $\epsilon$  (emissivity) is a measure of

how close the object's surface is to the ideal blackbody surface. If  $\epsilon = 1$ , the surface emits radiation (and absorbs radiation falling on it) like an ideal blackbody. For human skin, this value has been measured as approximately  $\epsilon = 0.98$ .<sup>4,8,9</sup> In other words, the human skin radiates energy almost like an ideal blackbody. Every blackbody emits energy itself as well as absorbs the energy emitted by the objects around it. If we take the ambient temperature as  $T_0$ , the energy taken from the environment is  $P_{absorbed} = \epsilon A\sigma T_0^4$ . Since the energy given and received is from the same surface, the net loss of energy per unit time from the human body to the surroundings by radiation is  $P_{net} = P_{emitted} - P_{absorbed} = \epsilon A\sigma(T^4 - T_0^4)$ . As the difference between the ambient temperature and the temperature of the human body increases, the heat loss by radiation also increases rapidly. Suppressing this radiation can reduce demand on energy for heating space around the human body to maintain thermal comfort. It has been shown that using a one-dimensional photonic crystal, we can suppress electromagnetic radiation (blackbody radiation).<sup>10</sup>

Photonic crystals (PCs) are artificially formed structures by periodic alternating arrangements of high and low dielectric constant materials.<sup>11–13</sup> When the waves reflect from this periodic structure, depending on the geometry of the periodic structure and the

27 February 2024 07:49:35

wavelength, waves scattered from different points of the structure cause interference, and depending on whether this interference is damping or strengthening gives rise to photonic bandgap (PBG) formation. Frequency falling into this gap is forbidden to propagate in the crystal. While the principle is so simple, the complexity of the geometry of the structure makes it difficult to determine without any prior calculations exactly what a given wave will do. While rough estimates are possible for some specific cases, in general, it is nearly impossible to predict the result with reasonable precision without doing some fairly intensive numerical calculations. Many calculations made in the late 1980s, when the interest in PCs first emerged, contained serious errors in this regard.<sup>14</sup>

Using vector nature of electromagnetic fields, the photonic band structure of a dielectric sphere arranged in face-centered-cubic (fcc) lattice symmetry is calculated for the first time.<sup>15</sup> Another three-dimensional structure that possesses a complete PBG is called “Yablonovite” and can be fabricated by chemical-beam-assisted ion etching.<sup>16</sup> The first three-dimensional photonic crystal with a complete bandgap is studied theoretically, which is called “woodpile,”<sup>17,18</sup> and fabricated using a “layer-by-layer” technique and experimentally studied in the microwave and far-infrared frequency regime.<sup>19,20</sup> Microwave transmittance values and band structures of a four-unit-cell thick photonic crystal formed from periodically stacked alumina rods were calculated.<sup>19</sup> Even with only four-unit-cell thickness, the transmittance for frequencies in the photonic bandgap decreased by  $-40$  to  $-70$  dB. In another pioneering study, the transmittance measurements of the fcc tetragonal photonic crystal, which consists of four periodically stacked layers, at frequencies between microwave and far infrared were examined,<sup>20</sup> and it was observed that the transmittance of the photonic crystal with four-unit-cell thickness decreased to around  $-50$  dB in the bandgap. In another work, the optical reflectivity dependence on the crystal thickness is studied, and it is shown that this dependence is weak and hardly increases with increasing thickness.<sup>21</sup> These results, especially the demonstration by Özbay that the microwave transmittance of a photonic crystal with a thickness of four unit cells can be reduced so much, gives us hope that photonic crystal thermal fabrics can be implemented practically.

Three-dimensional PC structures mentioned above are either hard to fabricate or fabrication methods are time consuming and expensive and the gaps obtained were in the microwave regime. For the human body at a temperature of  $37^\circ\text{C}$  (310 K), the wavelength at which radiation emitted at its maximum intensity is around  $10\ \mu\text{m}$ , but it has a very wide distribution and is in the infrared regime of the electromagnetic spectrum. Therefore, it is desirable to find an easy fabrication method for large-scale production with less time consumption with a fairly low cost.

Photonic bandgap properties of dielectric fibers woven into the three-dimensional structure, similar to weaving types used in textiles, that can behave as photonic crystals are calculated.<sup>22</sup> To obtain a wide bandgap, the dielectric constants of the fibers immersed in the air background need to be 40 (or greater). In a similar study, it is reported that an absolute photonic bandgap can be achieved with a fairly lower dielectric constant ( $\epsilon \sim 16$ ).<sup>23</sup> Topologically similar to previous two works, a large and robust photonic bandgap is achieved using square spiral posts in a tetragonal lattice.<sup>24,25</sup>

Using textile technology, a straight woodpile like fabric, a multilayered woven fabric, and a three-dimensional woven fabric were fabricated. It was shown that those structures possess a photonic bandgap in the 6–15 GHz range.<sup>26</sup> However, those structures are rigid and not suitable to change shape. Fibers formed from alumina balls into the teflon tube in a certain period as in photonic crystals<sup>27</sup> were fabricated. It was shown that flexible woven photonic crystals can be fabricated. Besides flexibility, a high dielectric contrast is also required for realization of a photonic bandgap. It was shown that the cotton-yarn coated by  $\text{TiO}_2$  can have a high dielectric contrast.<sup>28</sup> For high-temperature applications, the use of photonic crystal structures to control electromagnetic wave propagation of an object at temperatures around  $1000^\circ\text{C}$  (and above)<sup>29</sup> is proposed. However, since the wavelength will be  $3\ \mu\text{m}$  and below at these temperatures, the required fibers must be much finer.

Regulating thermal energy in the close vicinity of the human body without any input power, such as traditional heating and cooling systems, has attracted great interest in the scientific community. For cooling, materials used to make clothes need to be infrared-transparent visible-opaque to have a cooling effect. It was shown that synthetic polymer fibers,<sup>30</sup> nanoporous polyethylene (nanoPE),<sup>31,32</sup> boron nitride composite fibers (a-BN/PVA),<sup>33</sup> the nanofiber membrane (NFM),<sup>34</sup> the microstructure with randomly stacked silk fibers,<sup>35</sup> and nanoporous polymer matrix composites (PMCs)<sup>36</sup> are permeable to human body radiation in the mid-infrared spectrum but opaque to visible light. In another work, it was shown that using photonic crystal properties, woven, knitted, or nonwoven textiles<sup>37,38</sup> or polyethylene oxide films composed of random nanofibers as daytime radiative coolers<sup>39</sup> can be used to make effective cooling wearable clothes. It was shown that from high reflectance in the sunlight region because of its ordered or disordered photonic structure, selective emittance in the mid-infrared region can be achieved. A tri-layered structure [nylon (PA), polyvinylidene fluoride (PVDF), and polyethylene (PE)]<sup>40</sup> and hybrid membrane exfoliated BN nanosheets (BNNs) with layered double hydroxide (LDH) nanosheets covering the surface of the inorganic-organic hybrid cellulose membrane (ICM)<sup>41</sup> were studied for personal thermal management.

For heating purposes, a personal thermal management system based on a metallic nanowire-embedded fabric<sup>42</sup> and a fabricated MXene/nanoPE textile with a low IR emissivity at  $7\text{--}14\ \mu\text{m}$ <sup>43</sup> were proposed to reflect human body thermal radiation. Besides thermal insulation, this fabric can be supplied by power to have additional active heating functionality. Using nanoporous metallized polyethylene,<sup>44</sup> silk fibroin/graphene oxide aerogel fibers (SF/GO),<sup>45</sup> fibers composed of a polyurethane (PU)-ATO composite,<sup>46</sup> and carbon nanotubes (CNTs),<sup>47</sup> it was shown that the created nanophotonic structure textiles with tailored infrared (IR) properties can be used for passive personal heating. In another study, CNT/cellulose aerogel layers, cotton textiles, and copper nanowire (CuNW)-based conductive network (CNN) layers were used to create a laminated fabric with improved photothermal conversion, mid-infrared reflectance, thermal insulation, and electrical heating performance.<sup>48</sup>

Building energy efficiency and personal thermal management have both benefited from the development of dual-mode thermal management materials capable of both cooling and heating; for example, a bilayer emitter inserted inside an infrared-transparent

nanoporous polyethylene (nanoPE) layer in the dual-mode textiles can be used to perform both radiative cooling and heating.<sup>49</sup> By using engineered fabric building blocks, a metafabric was created and analyzed for applications, such as personal thermal cooling, thermal insulation, and thermoregulation.<sup>50</sup> Inspired from nature, a composite material inspired by squid skin's dynamic color-changing capability with tunable thermoregulatory capabilities was designed.<sup>51</sup> A polymer photonic membrane,<sup>52</sup> a nanostructured material<sup>53</sup> that captures solar energy, and dual-mode thermal management materials using just organic polymers<sup>54</sup> are studied with a view to thermoregulate the human body microclimate.

However, solutions proposed so far involve production of photonic crystals and somehow embedding them into or fixing them onto textiles. We observe that textiles, by virtue of the fact that it has been produced by weaving, already have a periodic structure and, thus, are a potential candidate for a photonic crystal. Thus, it is not necessary to manufacture a separate photonic crystal and somehow "mount" it on the textile. If the fiber that the textile is woven from has the necessary electrical, optical, and geometrical properties<sup>55</sup> and is woven with the right geometrical structure, then the textile itself would be a thin layer of photonic crystals.

## II. THEORY AND NUMERICAL METHODS

Source-free decoupled fully vectorial Maxwell's equation that governs the electromagnetic waves for both electric and magnetic fields can be written as

$$\vec{\nabla} \times \left[ \frac{1}{\mu(\vec{r})} \vec{\nabla} \times \vec{E}(\vec{r}) \right] = \left( \frac{\omega}{c} \right)^2 \epsilon(\vec{r}) \vec{E}(\vec{r}), \quad (1)$$

and a similar equation can be found for an electric field by replacing  $\epsilon(\vec{r}) \leftrightarrow \mu(\vec{r})$  and  $\vec{H} \leftrightarrow \vec{E}$ ,

$$\vec{\nabla} \times \left[ \frac{1}{\epsilon(\vec{r})} \vec{\nabla} \times \vec{H}(\vec{r}) \right] = \left( \frac{\omega}{c} \right)^2 \mu(\vec{r}) \vec{H}(\vec{r}), \quad (2)$$

and the Fourier transformed form using a plane-wave basis can be written as  $\vec{H}_{\vec{k}}(\vec{r}) = e^{i\vec{k}\cdot\vec{r}} \vec{u}_{\vec{k}}(\vec{r})$ , where  $\vec{u}_{\vec{k}}(\vec{r})$ , the periodic function, subject to the transversality condition is defined as  $(i\vec{k} + \vec{\nabla}) \cdot \vec{u}_{\vec{k}}$ ,

$$\sum_{\vec{G}} \zeta(\vec{G} - \vec{G}') (\vec{k} + \vec{G}) \times \left[ (\vec{k} + \vec{G}') \times \vec{E}(\vec{k} + \vec{G}') \right] + \frac{\omega^2}{c^2} \sum_{\vec{G}} \epsilon(\vec{G} - \vec{G}') \vec{E}(\vec{k} + \vec{G}') = 0. \quad (3)$$

A similar equation for the magnetic field,  $\vec{H}$ , is obtained by substitution  $\vec{E} \rightarrow \vec{H}$ ,  $\epsilon \rightarrow \mu$ , and  $\zeta \rightarrow \eta$ .

$$\sum_{\vec{G}} \eta(\vec{G} - \vec{G}') (\vec{k} + \vec{G}) \times \left[ (\vec{k} + \vec{G}') \times \vec{H}(\vec{k} + \vec{G}') \right] + \frac{\omega^2}{c^2} \sum_{\vec{G}} \mu(\vec{G} - \vec{G}') \vec{H}(\vec{k} + \vec{G}') = 0. \quad (4)$$

Fully vectorial eigenmodes of Maxwell's equations with periodic

boundary conditions were computed by preconditioned conjugate-gradient minimization of the block Rayleigh quotient on a plane-wave basis using freely available software package MPB.<sup>56</sup>

### A. Finite-difference time-domain method

The propagation of electromagnetic waves, namely, Maxwell's equation in the time domain, can be written as

$$\frac{\partial \vec{H}}{\partial t} = -\frac{1}{\mu} (\vec{M}_s + \sigma^* \vec{H}) - \frac{1}{\mu} \vec{\nabla} \times \vec{E}, \quad (5)$$

$$\frac{\partial \vec{E}}{\partial t} = -\frac{1}{\epsilon} (\vec{J}_s + \sigma \vec{E}) + \frac{1}{\epsilon} \vec{\nabla} \times \vec{H}, \quad (6)$$

where the magnetic flux density  $\vec{B}$  and the displacement field  $\vec{D}$  are defined as  $\vec{B} = \mu \vec{H}$  and  $\vec{D} = \epsilon \vec{E}$ , respectively. The current density of the electric charge is denoted by  $\vec{J}_s$ , and the magnetic current density is denoted by  $\vec{M}_s$ . The remaining terms denoted by  $\sigma^*$  and  $\sigma$  are magnetic and electric conductivities. We differentiate both Eqs. (5) and (6) and writing the components explicitly for the magnetic field,

$$\frac{\partial H_x}{\partial t} = \frac{1}{\mu} \left[ \frac{\partial E_y}{\partial z} - \frac{\partial E_z}{\partial y} - (M_{sx} + \sigma^* H_x) \right], \quad (7)$$

$$\frac{\partial H_y}{\partial t} = \frac{1}{\mu} \left[ \frac{\partial E_z}{\partial x} - \frac{\partial E_x}{\partial z} - (M_{sy} + \sigma^* H_y) \right], \quad (8)$$

$$\frac{\partial H_z}{\partial t} = \frac{1}{\mu} \left[ \frac{\partial E_x}{\partial y} - \frac{\partial E_y}{\partial x} - (M_{sz} + \sigma^* H_z) \right], \quad (9)$$

and for the electric field,

$$\frac{\partial E_x}{\partial t} = \frac{1}{\epsilon} \left[ \frac{\partial H_z}{\partial y} - \frac{\partial H_y}{\partial z} - (J_{sx} + \sigma E_x) \right], \quad (10)$$

$$\frac{\partial E_y}{\partial t} = \frac{1}{\epsilon} \left[ \frac{\partial H_x}{\partial z} - \frac{\partial H_z}{\partial x} - (J_{sy} + \sigma E_y) \right], \quad (11)$$

$$\frac{\partial E_z}{\partial t} = \frac{1}{\epsilon} \left[ \frac{\partial H_y}{\partial x} - \frac{\partial H_x}{\partial y} - (J_{sz} + \sigma E_z) \right]. \quad (12)$$

These equations can be solved using the finite-difference time-domain (FDTD) method to obtain the transmission spectrum or the response of a medium to a given pulse. The transmission spectrum as a function of frequency is obtained by employing FDTD, which calculates the response of a material to a short pulse source by simulation in the time domain. To solve these equations numerically, Yee introduced an algorithm<sup>57</sup> that uses a central difference for a derivative of fields in time and space variables.

Time domain simulations were performed with the FDTD method<sup>58,59</sup> using open-source software package Meep.<sup>60</sup> Meep uses a perfectly matched layer<sup>61</sup> (PML) as an absorber of electromagnetic waves for open boundary problems. The current source

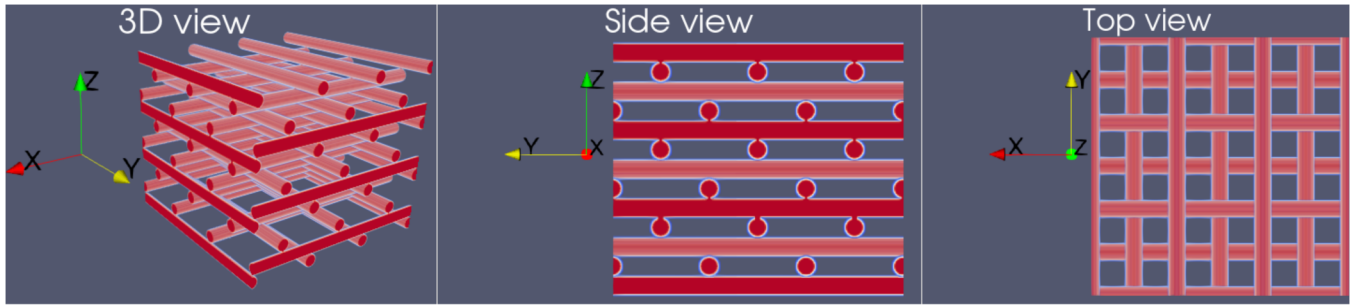


FIG. 1. 3D view: Three-dimensional woodpile photonic crystal made of cylindrical rods. Lattice constant along  $x$  and  $y$  directions are  $a_x = a_y = a$  and along the  $z$  direction is  $a_z = 8r$ , where  $r$  is the radius of cylindrical rods. Side view: View from the  $yz$  plane. Top view: View from the  $xy$  plane.

utilized in our simulation is expressed as the multiplication of a spatial function with a temporal function. The mathematical expression is given by  $\vec{J}(\vec{r}, t) = \vec{A}(\vec{r})f(t)$ , where  $\vec{A}(\vec{r}) = C\delta(z - z_0)$  and  $f(t) = Ce^{(-i\omega t - (t-t_0)^2/2w^2)}$ .

The radiation model we used is based on the fact that the transmissions are dimensionless quantities; therefore, we first calculated the normalized transmitted flux spectrum and then multiplied the transmission values by the blackbody spectrum, which is defined as  $B(\nu, T) = (4\pi h/c^2)\nu^3/(e^{h\nu/kT} - 1)$  (spectral radiance, units of  $W m^{-2} s^{-1}$ ), to obtain transmitted power by the proposed structure.

### B. Bare woodpile photonic crystal structure

The first structure we used in this work is the usual three-dimensional (3D) woodpile photonic crystal, which we refer to as the bare woodpile photonic crystal. As shown in Fig. 1, cylindrical rods are stacked on top of each other along the stacking direction,  $z$ -direction. In each layer, the cylindrical rods in the adjacent layers are rotated so that their symmetry axis makes  $90^\circ$  angle with respect to each other. In addition, each layer is shifted by half of a unit cell, and cylindrical rods are separated by a lattice constant  $a$  in both  $x$  and  $y$  directions. Repeating this way after the fourth layer, the structure starts to repeat itself along the stacking direction, and one can construct a unit cell along the  $z$  axis that has a thickness of  $a_z = 8r$ , where  $r$  is the radius of cylindrical rods. In all calculations, the lattice constant along  $x$  and  $y$  directions is taken to be  $a_x = a_y = a = 1$ , and the dielectric constant of cylindrical rods is taken to be  $\epsilon_a = 5.38$ , which corresponds to Kevlar's dielectric constant, while the background material is taken to be  $\epsilon_b = 1.00$ , which corresponds to air (vacuum). The volume of the unit cell is  $V_{cell} = a_x \times a_y \times a_z = a \times a \times 8r$ . The band calculations are done using 64 resolution, which is good enough to get accurate results.

To optimize the photonic bandgap, we performed a scan of the radius from  $r = 0.140a$  to  $r = 0.180a$  and calculated the ratio of the bandgap to the midgap frequency. The resulting gap-midgap ratio was then plotted as a function of the cylinder radius to the lattice constant ( $r/a$ ), as shown in Fig. 2 (left). For the optimum values, we have also shown the photonic band structure along the  $\Gamma - X$  direction in Fig. 2 (right). The maximum gap is achieved for radius  $r = 0.145a$ . For this radius and dielectric constant, it is about 28.68%.

In order to see the potential of the proposed structure in principle, we first calculated the amount of the electromagnetic energy moving perpendicular to this structure transmitted to the other side of the bare woodpile structure. For normalization of the total energy, we need to calculate the amount of energy radiated by the source first, then introduce the structure, and recalculate the

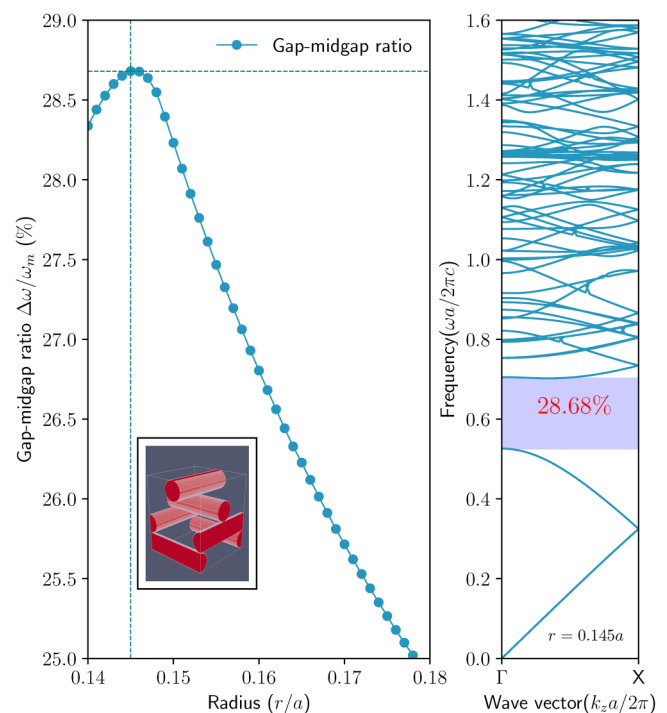
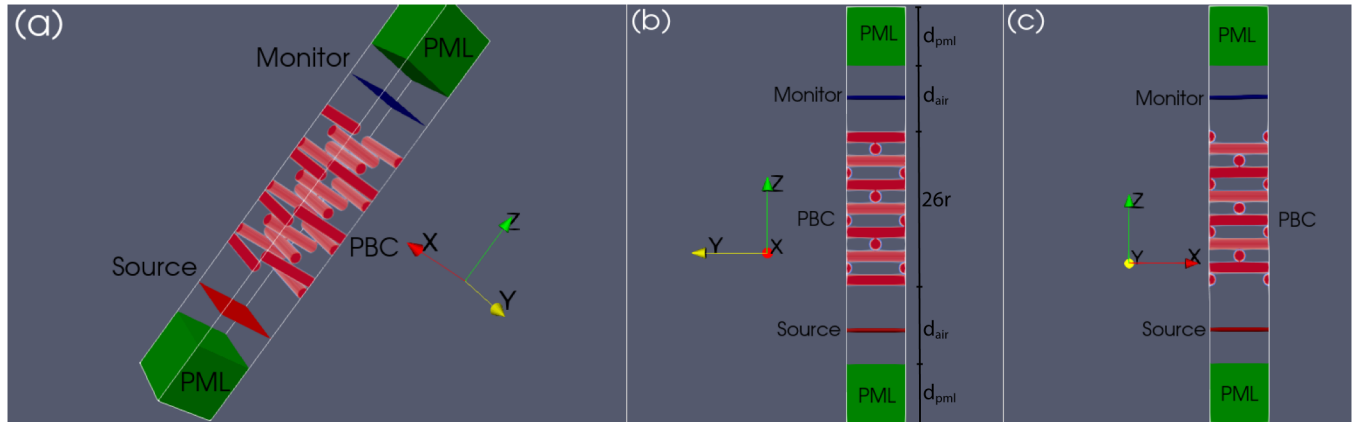


FIG. 2. Left figure is a gap-midgap ratio graph as a function of  $r/a$ . The maximum value of the gap-midgap ratio is achieved for  $r/a = 0.145$ . The dielectric constant of circular rods is taken to be  $\epsilon_a = 5.38$ , and the dielectric constant of the background is  $\epsilon_b = 1.00$  (air). The right figure is the calculated photonic band structure for  $r/a = 0.145$  along the propagation direction, which is chosen to be along the  $\Gamma - X$  direction.

27 February 2024 07:49:35





**FIG. 3.** The simulation setup that is used to calculate the transmission spectrum. Three-dimensional bare woodpile structures made by a single unit cell along  $x$  and  $y$  directions. In the third direction, we used three unit cells and added one extra layer so that it is made symmetric. The green region is the PML boundary that mimics the illusion of the open boundary. In  $x$  and  $y$  directions, periodic boundary conditions (PBCs) are used. The computational cell volume is  $1a \times 1a \times 20a$ , where  $a$  is a lattice constant. (a) Three-dimensional view. (b)  $yz$ -plane view.  $d_{pml} = 5a$  is the thickness of the PML region,  $d_{air} = 3a$  is the air region, and the thickness of the structure is  $26r$ . (c)  $xz$ -plane view.

amount of energy that passes the structure. To do so, two separate calculations are performed: one without a structure (vacuum only) and one with a structure introduced.

The structure we use in transmission calculations is shown in Fig. 3. We used periodic boundary conditions (PBCs) in the  $xy$  direction and a perfectly matched layer (PML) in the  $z$  direction, which is the propagation direction. The simulation cell is taken to be one unit cell in the  $x$  and  $y$  direction, while in the  $z$  direction, a three unit cell is used. An extra cylinder is put at the far side of the source so that the structure is symmetric along the stacking direction. The purpose of the extra cylinder will be more clear in Sec. II C when we connect the cylinders. The volume of the computational cell is  $V_{comp-cell} = S_x \times S_y \times S_z = a \times a \times 20a$ . The resolution of the computational grid is taken to be 64 along each direction ( $64 \times 64 \times 1280$ ). The thickness of the PML is taken to be  $5a$  to get good convergence in a reasonable amount of run time.

In what follows, we used a normalized frequency defined as  $f \equiv \omega a / 2\pi c$ . A gaussian pulse with a bandwidth of  $\Delta f = 1.5$  and a center frequency  $f = 0.85$  is used to excite the  $x$  component of the electric field, ( $E_x$ ), which propagates along the stacking direction ( $z$  direction) with the frequency ranging from  $f = 0.10$  to  $f = 1.60$ . The number of frequency that is used to sample the spectrum is taken to be 9000, which is good enough to sample this bandwidth. The calculated transmission spectrum of the bare woodpile structure is shown in Fig. 4 (top). The shaded area shows the bandgap region.

The black curve in Fig. 4 (bottom) is the blackbody radiation curve as a function of frequency. For different temperatures, the peak value of the curve will change accordingly. For an object at temperature  $T = 310$  K, which is the skin temperature of the human body, the peak value of this curve is around 18.22 THz. By scaling the peak value of the blackbody curve to the center frequency of the bandgap, we can get an idea about the proposed

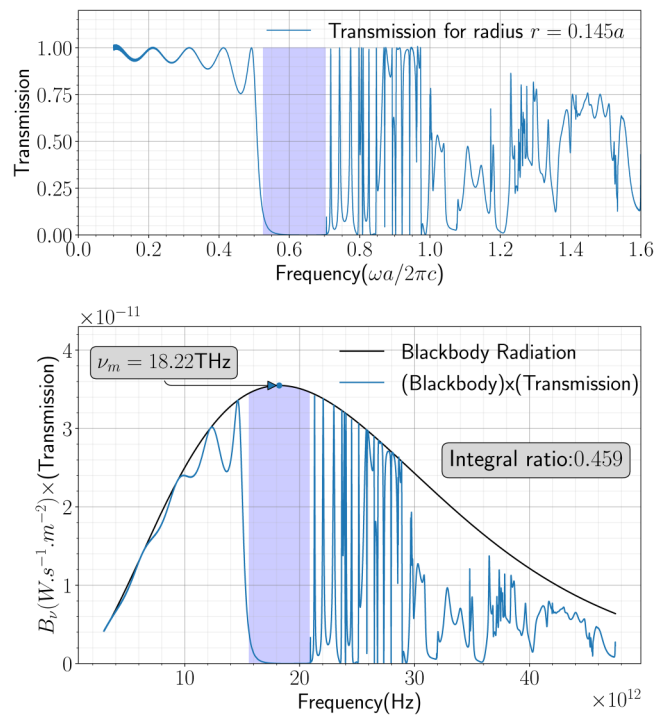


**FIG. 4.** Top figure is the normalized transmission spectrum of the bare woodpile structure as a function of frequency. The bottom graph is the transmission spectrum of the bare woodpile multiplied by blackbody radiation. The blackbody radiation spectrum of an object at a temperature of 310 K. The spectrum has the maximum radiation peak around 18.22 THz. The transmission graph for the woodpile photonic crystal.

27 February 2024 07:49:35

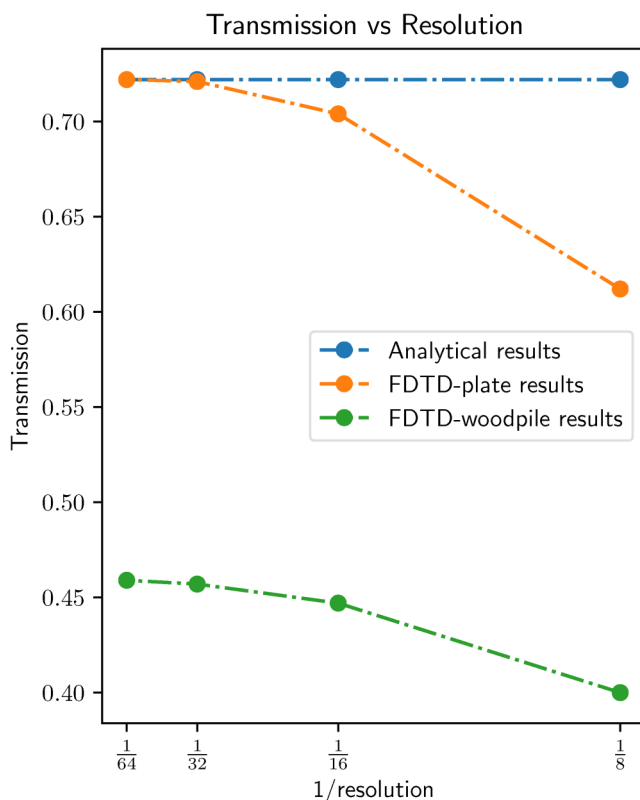


**FIG. 5.** Transmission values vs inverse of resolution. The blue curve is the analytical result, and the orange line is the FDTD simulation result for a homogeneous plate. The green line is FDTD simulation results of the bare woodpile structure.

structure ability of blocking electromagnetic radiation. The blue curve in Fig. 4 (bottom) shows that the blackbody radiation spectrum of the structure, which is obtained by multiplying the transmission values by the spectrum of blackbody radiation, is interesting in that it shows what kind of results we can expect. The

area under each curve represents the total energy. When we proportioned these areas, we found that the so-called bare woodpile reflects back about 55% of the energy. Since the thickness of the structure is finite, there will be slight transmission even at a frequency in the bandgap calculated for the infinite structure.

To validate the numerical method, we calculated transmission values of a single layer homogeneous plate for which the analytical solution is known. Analytical and numerical results of the homogeneous plate are shown in Fig. 5 (blue and orange curves, respectively). Transmission values vs resolution of the woodpile structure are also shown in Fig. 5 (green curve). As a convergence check, the simulations were performed with four different grid resolution values: 8, 16, 32, and 64. The percentage of the transmitted energy for each resolution is found to be 40%, 44.7%, 45.7%, and 45.9%, respectively, which indicates that even with a resolution of 32, the results are converged. The stopping condition for the termination of simulation is based on the total energy within the computational volume. We monitor the total energy within the entire volume, and the simulation continues until the specified ( $10^{-4}$ ) level of accuracy is achieved.

### C. Textile-like woven woodpile photonic crystal structure

The bare woodpile structure is simple to make, but it is not rigid to use as a textile. To make it more robust, we have connected cylindrical rods using thinner yarns. Those yarns are woven along the single direction (along the  $x$  direction in this case). Their radii are chosen to be as thin as possible so that they do not affect the photonic bandgap of the structure too much. The structure is constructed by connecting every three layers along the  $z$ -axis using yarns that are extending along the  $x$ -axis. Cylindrical rods extending along the  $y$  axis are connected to each other with yarns extending along the  $x$  axis with smaller radii. The radius of connection lines is  $r_c = r/4$ , where  $r$  is the radius of cylinders of a woodpile structure. The resulting structure is shown in Fig. 6 for the three unit cell along each direction.

To compare the performance of the woven structure with the bare structure, we calculated the transmission of electromagnetic radiation from the constructed structure. We used the computational volume shown in Fig. 7 with periodic boundary conditions

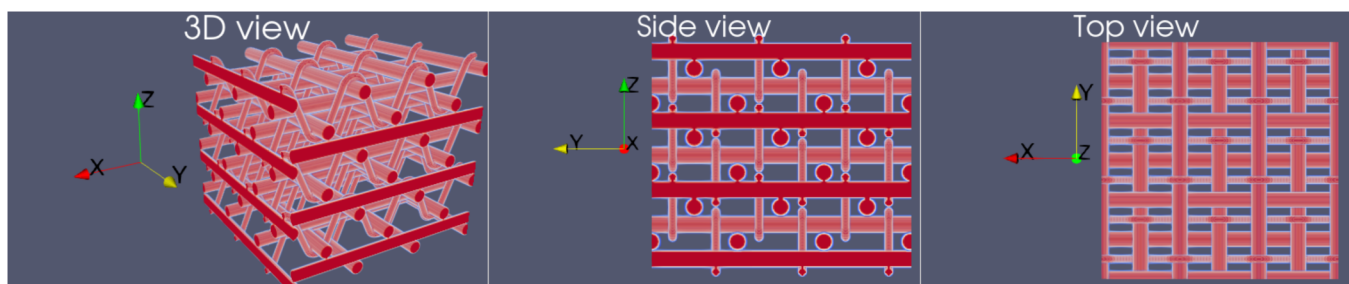


**FIG. 6.** 3D view: Textile-like woven woodpile photonic crystal. Cylinder with a radius of  $r/a = 0.145$  and the connecting yarns having a radius of  $r_c = r/4$  are used. The structure is immersed in an air background, while the dielectric constant of cylinders is taken to be  $\epsilon_a = 5.38$ . Side view: View from the  $yz$  plane. Top view: View from the  $xy$  plane.

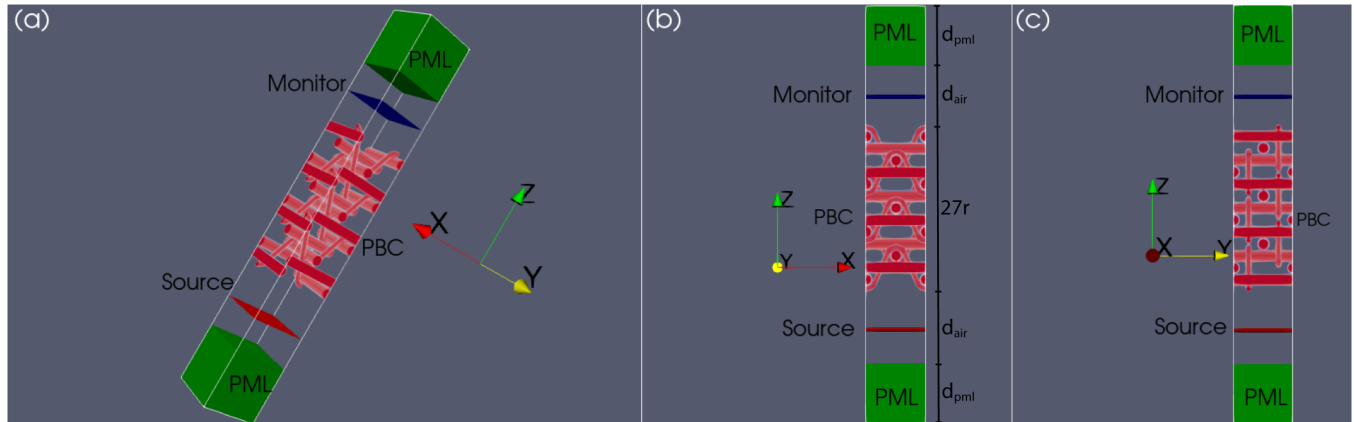


**FIG. 7.** Simulation setup used for transmission calculations. Dielectric constant of cylinders and connecting yarns are taken to be the same ( $\epsilon_a = 5.34$ ). The structure is immersed in the air background  $\epsilon_b = 1.00$ . The radii of cylinders are the same with the bare woodpile ( $r/a = 0.145$ ). The radius of connecting yarns is  $r_c = r/4a$ . (a) Three-dimensional view. (b)  $xz$ -plane view.  $d_{pml} = 5a$  is the thickness of the PML region,  $d_{air} = 3a$  is the air region, and the thickness of the structure is  $27r$ . (c)  $yz$ -plane view.

applied in  $x$  and  $y$  directions. For the propagation direction, the  $z$  direction, we implemented an open boundary using PML. In the simulations, three unit cells are used in the propagation direction ( $z$  direction), while a single unit cell is used in  $x$  and  $y$  directions. As in Sec. II B, we again used a two-dimensional plane-wave source to excite a gaussian-profiled pulse with the frequency ranging from 0.10 to 1.60 centered at 0.85. To capture the flux that has passed the structure, we placed a monitor on the opposite side. After a sufficient amount of run time, the captured flux is calculated.

In Fig. 8, two graphs are presented. The top graph displays the calculated transmission values for the woven woodpile structure. The bottom graph shows the blackbody radiation curve (in black) and transmission values multiplied by blackbody radiation (in blue). To obtain the blue curve, we first scaled the transmission values so that the mid-gap frequency coincided with the maximum of the blackbody radiation curve since most of the energy is concentrated around this point. This is done to ensure that the blue curve represents the amount of radiation that would be transmitted through the woven structure if it were exposed to blackbody radiation at the same temperature as the curve. The resulting curve represents the fraction of blackbody radiation that would be transmitted through the woven structure at different frequencies.

The area under the black curve is the total energy radiated by a blackbody, while the area under the blue curve gives the total energy that would be transmitted through the structure. If we calculate the ratio of the total areas under the graphs, we find that the woven structure blocks approximately 53% of electromagnetic radiation. The transmission calculations are done using the structure with finite thickness, and since the full PBG is only possible for crystals that have an infinite extent, the calculated transmission results, of course, would be different from the expected ones. For maximum reflection (and minimum transmission), it is desired to have a bandgap as wide as possible. This is because a wide bandgap allows the photonic crystal to block a greater range of frequencies, particularly those centered around the maximum value of the blackbody curve. By preventing the transmission of these frequencies, the photonic crystal

can effectively reflect and scatter the incident light, resulting in a high degree of optical confinement within the structure.

These results can further be improved by optimizing the kind of material and the geometric parameters, such as dielectric

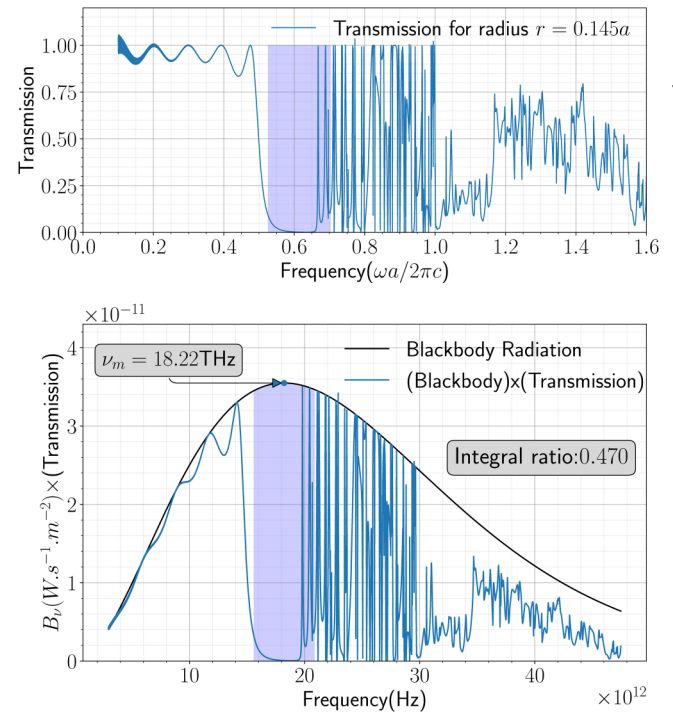


**FIG. 8.** Transmission graph for the textile-like woven woodpile structure (top). Blackbody radiation spectrum at 310 K (black curve). Transmission values multiplied by the blackbody spectrum (bottom blue curve).

27 February 2024 07:49:35



constants. Increasing the dielectric value will increase the bandgap of the structure so that the transmitted amount of energy will decrease.

### III. RESULTS AND DISCUSSION

In this work, we addressed the problem of heat loss from the human body. Under normal conditions, the amount of heat lost through electromagnetic radiation from the human body skin accounts for about two-thirds of the total energy produced by the human body. Therefore, suppressing this energy can save a substantial amount of power used to heat the human body's environment. The main contribution of our work is to use photonic crystals' (PhCs) ability to confine electromagnetic radiation to produce woven textiles that can be considered a thin layer of the electromagnetic shield. Depending on the kind of application, the amount of energy that passes the structure can be tuned. For isolation purposes, a wider bandgap is desirable. On the other hand, for cooling purposes, a material without a bandgap would be ideal. By using a three-dimensional structure called "bare woodpile" and "woven woodpile" PhC that is known for its complete photonic bandgap, we have shown that it is possible to reduce heat loss.

The degrees of freedom of the problem are those that would affect the PBG. Those are the dielectric constant, the thickness of the yarn, and the weaving pattern. In simulations, we assumed that the dielectric constant of the structures is real-symmetric and frequency-independent. Then, we used a moderate frequency independent dielectric constant so that we could create a contrast between the material and the background. As a material property, we used a real dielectric constant, which means that no gain or loss occurs. However, for more realistic calculations, it is necessary to use the real and imaginary parts of the dielectric function of the material that the textile/structure is made of. Although this approach will considerably increase the computational burden, it will also improve the accuracy of the calculations. The dielectric material used in calculations is assumed to be isotropic, which means that the material threat due to electromagnetic radiation is the same in all directions. However, most of the materials used in the textile industry are anisotropic. The inclusion of this effect will help us develop models that provide us with more realistic results.

Leaving those aside, we are left with two degrees of freedom, namely, the radius of the yarns and the weave pattern. We used a woodpile structure made of cylindrical rods as the weaving pattern and optimized it to obtain the maximum bandgap that one can get with that moderate value of dielectric constant,  $\epsilon_a = 5.38$ . The optimized structure radius is found to be  $r = 0.145a$ , where  $a$  is the lattice constant. The lattice constant can be calculated using  $a = c\tilde{f}/f_{peak}$ , where  $c$  is the speed of light and  $\tilde{f}$  is the normalized frequency,  $f = 0.85$ . At 310 K, the peak frequency,  $f_{peak}$ , of radiation is around  $f_{peak} = 18.22$  THz. This gives  $a = 14\mu\text{m}$ ; therefore, the diameter of the yarn is  $d = 2r = 4.06\mu\text{m}$ .

The source we used in our calculation is a gaussian-profiled plane wave spanning two dimensions. To get more realistic results, we need to represent the blackbody radiation spectrum by using randomly oriented dipoles that would radiate in all directions.

We also disregarded absorption due to radiation from the environment. Thus, our results are valid for extremely cold

environments. Taking the absorption from environment into account would enable optimal design for different environmental conditions, such as out in the sun or at home or at a moderate cold temperature around  $0^\circ\text{C}$ . Furthermore, the bandgap can be fine-tuned so that absorption from the environment can be made less than the radiation to the environment for a cooling effect.

Even though we mainly aimed to find the optimum woven structure that maximizes the reflection of radiation from an object at  $37^\circ\text{C}$ , the same approach, in principle, can be used to find structures that reflect radiation emitted by objects at higher temperatures, such as those that firefighters might be exposed to. In principle, this method can be scaled to any regime of the electromagnetic spectrum, except for the regimes that have very high energy and might destroy the molecular structure of the material.

### ACKNOWLEDGMENTS

The numerical calculations reported in this paper were fully performed at TUBITAK ULAKBIM, High Performance and Grid Computing Center (TRUBA resources).

### AUTHOR DECLARATIONS

#### Conflict of Interest

The authors have no conflicts to disclose.

#### Author Contributions

**Zebih Çetin:** Formal analysis (equal); Software (equal); Writing – original draft (equal). **Yiğit Tunçtürk:** Software (equal). **H. Sami Sözüer:** Conceptualization (equal); Project administration (equal); Supervision (equal).

### DATA AVAILABILITY

Data sharing is not applicable to this article as no new data were created or analyzed in this study.

### REFERENCES

- <sup>1</sup>J. D. Hardy *et al.*, "The radiation of heat from the human body: I. An instrument for measuring the radiation and surface temperature of the skin," *J. Clin. Investig.* **13**, 593–604 (1934).
- <sup>2</sup>J. D. Hardy *et al.*, "The radiation of heat from the human body: II. A comparison of some methods of measurement," *J. Clin. Investig.* **13**, 605–614 (1934).
- <sup>3</sup>J. D. Hardy *et al.*, "The radiation of heat from the human body: III. The human skin as a black-body radiator," *J. Clin. Investig.* **13**, 615–620 (1934).
- <sup>4</sup>J. D. Hardy, C. Muschenheim *et al.*, "The radiation of heat from the human body. IV. The emission, reflection, and transmission of infra-red radiation by the human skin," *J. Clin. Investig.* **13**, 817–831 (1934).
- <sup>5</sup>C.-E. Winslow, A. Gagge, and L. Herrington, "The influence of air movement upon heat losses from the clothed human body," *Am. J. Physiol.* **127**, 505–518 (1939).
- <sup>6</sup>J. D. Hardy and E. F. DuBois, "Regulation of heat loss from the human body," *Proc. Natl. Acad. Sci. U.S.A.* **23**, 624 (1937).
- <sup>7</sup>M. Planck, *The Theory of Heat Radiation* (CreateSpace Independent Publishing Platform, 2013).
- <sup>8</sup>F. J. Sanchez-Marin, S. Calixto-Carrera, and C. Villaseñor-Mora, "Novel approach to assess the emissivity of the human skin," *J. Biomed. Opt.* **14**, 024006 (2009).

- <sup>9</sup>J. Steketee, "Spectral emissivity of skin and pericardium," *Phys. Med. Biol.* **18**, 686 (1973).
- <sup>10</sup>C. M. Cornelius and J. P. Dowling, "Modification of Planck blackbody radiation by photonic band-gap structures," *Phys. Rev. A* **59**, 4736 (1999).
- <sup>11</sup>S. John, "Strong localization of photons in certain disordered dielectric superlattices," *Phys. Rev. Lett.* **58**, 2486 (1987).
- <sup>12</sup>E. Yablonovitch, "Inhibited spontaneous emission in solid-state physics and electronics," *Phys. Rev. Lett.* **58**, 2059 (1987).
- <sup>13</sup>E. Yablonovitch and T. Gmitter, "Photonic band structure: The face-centered-cubic case," *Phys. Rev. Lett.* **63**, 1950 (1989).
- <sup>14</sup>H. S. Sözüer, J. Haus, and R. Inguva, "Photonic bands: Convergence problems with the plane-wave method," *Phys. Rev. B* **45**, 13962 (1992).
- <sup>15</sup>K. Ho, C. T. Chan, and C. M. Soukoulis, "Existence of a photonic gap in periodic dielectric structures," *Phys. Rev. Lett.* **65**, 3152 (1990).
- <sup>16</sup>E. Yablonovitch, T. Gmitter, and K.-M. Leung, "Photonic band structure: The face-centered-cubic case employing nonspherical atoms," *Phys. Rev. Lett.* **67**, 2295 (1991).
- <sup>17</sup>H. Sözüer and J. P. Dowling, "Photonic band calculations for woodpile structures," *J. Mod. Opt.* **41**, 231–239 (1994).
- <sup>18</sup>K. M. Ho, C. T. Chan, C. M. Soukoulis, R. Biswas, and M. Sigalas, "Photonic band gaps in three dimensions: New layer-by-layer periodic structures," *Solid State Commun.* **89**, 413–416 (1994).
- <sup>19</sup>E. Özbay, A. Abeysa, G. Tuttle, M. Tringides, R. Biswas, C. T. Chan, C. M. Soukoulis, and K. Ho, "Measurement of a three-dimensional photonic band gap in a crystal structure made of dielectric rods," *Phys. Rev. B* **50**, 1945 (1994).
- <sup>20</sup>E. Özbay, "Layer-by-layer photonic crystals from microwave to far-infrared frequencies," *JOSA B* **13**, 1945–1955 (1996).
- <sup>21</sup>T. Tajiri, S. Takahashi, C. A. Harteveld, Y. Arakawa, S. Iwamoto, and W. L. Vos, "Reflectivity of three-dimensional GaAs photonic band-gap crystals of finite thickness," *Phys. Rev. B* **101**, 235303 (2020).
- <sup>22</sup>Y.-C. Tsai, K. W. Shung, and J. B. Pendry, "Three-dimensional photonic band gaps in woven structures," *J. Phys.: Condens. Matter* **10**, 753 (1998).
- <sup>23</sup>Y.-C. Tsai, J. B. Pendry, and K. W.-K. Shung, "Absolute three-dimensional photonic band gap in the infrared regime in woven structures," *Phys. Rev. B* **59**, R10401 (1999).
- <sup>24</sup>O. Toader and S. John, "Proposed square spiral microfabrication architecture for large three-dimensional photonic band gap crystals," *Science* **292**, 1133–1135 (2001).
- <sup>25</sup>R. L. Chern, C. Chung Chang, C. C. Chang, and R. R. Hwang, "Numerical study of three-dimensional photonic crystals with large band gaps," *J. Phys. Soc. Jpn.* **73**, 727–737 (2004).
- <sup>26</sup>Y. Watanabe, T. Kobayashi, S. Kirihara, Y. Miyamoto, and K. Sakoda, "Cotton-yarn/TiO<sub>2</sub> dispersed resin photonic crystals with straight and wavy structures," *Eur. Phys. J. B* **39**, 295–300 (2004).
- <sup>27</sup>Y. Watanabe, T. Hotta, and H. Sato, "Fabrication of flexible photonic crystal using alumina ball inserted teflon tube," *Appl. Phys. A* **100**, 981–985 (2010).
- <sup>28</sup>M. Furukawa, H. Sato, and Y. Watanabe, "Fabrication of TiO<sub>2</sub> coated cotton-yarn as high-dielectric-constant fiber for 3-D photonic crystal application," *Trans. Mater. Res. Soc. Jpn.* **37**, 35–38 (2012).
- <sup>29</sup>V. Shklover, L. Braginsky, M. Mishrikey, and C. Hafner, "High-temperature fiber matrix composites for reduction of radiation heat transfer," *MRS Online Proc. Lib.* **1162**, 1–6 (2009).
- <sup>30</sup>J. K. Tong, X. Huang, S. V. Boriskina, J. Loomis, Y. Xu, and G. Chen, "Infrared-transparent visible-opaque fabrics for wearable personal thermal management," *ACS Photonics* **2**, 769–778 (2015).
- <sup>31</sup>P.-C. Hsu, A. Y. Song, P. B. Catrysse, C. Liu, Y. Peng, J. Xie, S. Fan, and Y. Cui, "Radiative human body cooling by nanoporous polyethylene textile," *Science* **353**, 1019–1023 (2016).
- <sup>32</sup>L. Cai, Y. Peng, J. Xu, C. Zhou, C. Zhou, P. Wu, D. Lin, S. Fan, and Y. Cui, "Temperature regulation in colored infrared-transparent polyethylene textiles," *Joule* **3**, 1478–1486 (2019).
- <sup>33</sup>T. Gao, Z. Yang, C. Chen, Y. Li, K. Fu, J. Dai, E. M. Hitz, H. Xie, B. Liu, J. Song, and B. Yang, "Three-dimensional printed thermal regulation textiles," *ACS Nano* **11**, 11513–11520 (2017).
- <sup>34</sup>R. Xiao, C. Hou, W. Yang, Y. Su, Y. Li, Q. Zhang, P. Gao, and H. Wang, "Infrared-radiation-enhanced nanofiber membrane for sky radiative cooling of the human body," *ACS Appl. Mater. Interfaces* **11**, 44673–44681 (2019).
- <sup>35</sup>Z. Yang and J. Zhang, "Bioinspired radiative cooling structure with randomly stacked fibers for efficient all-day passive cooling," *ACS Appl. Mater. Interfaces* **13**, 43387–43395 (2021).
- <sup>36</sup>K. Zhou, W. Li, B. B. Patel, R. Tao, Y. Chang, S. Fan, Y. Diao, and L. Cai, "Three-dimensional printable nanoporous polymer matrix composites for daytime radiative cooling," *Nano Lett.* **21**, 1493–1499 (2021).
- <sup>37</sup>P. B. Catrysse, A. Y. Song, and S. Fan, "Photonic structure textile design for localized thermal cooling based on a fiber blending scheme," *ACS Photonics* **3**, 2420–2426 (2016).
- <sup>38</sup>M. Chen, D. Pang, J. Mandal, X. Chen, H. Yan, Y. He, N. Yu, and Y. Yang, "Designing mesoporous photonic structures for high-performance passive daytime radiative cooling," *Nano Lett.* **21**, 1412–1418 (2021).
- <sup>39</sup>D. Li, X. Liu, W. Li, Z. Lin, B. Zhu, Z. Li, J. Li, B. Li, S. Fan, J. Xie, and J. Zhu, "Scalable and hierarchically designed polymer film as a selective thermal emitter for high-performance all-day radiative cooling," *Nat. Nanotechnol.* **16**, 153–158 (2021).
- <sup>40</sup>Y.-N. Song, Y. Li, D.-X. Yan, J. Lei, and Z.-M. Li, "Novel passive cooling composite textile for both outdoor and indoor personal thermal management," *Compos. Part A: Appl. Sci. Manuf.* **130**, 105738 (2020).
- <sup>41</sup>B. Gu, H. Zhou, Z. Zhang, T. Zhang, M. Chen, F. Qiu, and D. Yang, "Cellulose-based hybrid membrane with functional integration for personal thermal management applications," *Appl. Surf. Sci.* **535**, 147670 (2021).
- <sup>42</sup>P.-C. Hsu, X. Liu, C. Liu, X. Xie, H. R. Lee, A. J. Welch, T. Zhao, and Y. Cui, "Personal thermal management by metallic nanowire-coated textile," *Nano Lett.* **15**, 365–371 (2015), PMID: 25434959.
- <sup>43</sup>M. Shi, M. Shen, X. Guo, X. Jin, Y. Cao, Y. Yang, W. Wang, and J. Wang, "Ti<sub>3</sub>C<sub>2</sub>T<sub>x</sub> mxene-decorated nanoporous polyethylene textile for passive and active personal precision heating," *ACS Nano* **15**, 11396–11405 (2021).
- <sup>44</sup>L. Cai, A. Y. Song, P. Wu, P.-C. Hsu, Y. Peng, J. Chen, C. Liu, P. B. Catrysse, Y. Liu, A. Yang, and C. Zhou, "Warming up human body by nanoporous metalized polyethylene textile," *Nat. Commun.* **8**, 1–8 (2017).
- <sup>45</sup>Z. Wang, H. Yang, Y. Li, and X. Zheng, "Robust silk fibroin/graphene oxide aerogel fiber for radiative heating textiles," *ACS Appl. Mater. Interfaces* **12**, 15726–15736 (2020).
- <sup>46</sup>S.-M. Jeong, J. Ahn, Y. K. Choi, T. Lim, K. Seo, T. Hong, G. H. Choi, H. Kim, B. W. Lee, S. Y. Park, and S. Ju, "Development of a wearable infrared shield based on a polyurethane-antimony tin oxide composite fiber," *NPG Asia Mater.* **12**, 32 (2020).
- <sup>47</sup>H. Yu, X. Yang, Y. Lian, M. Wang, Y. Liu, Z. Li, Y. Jiang, and J. Gou, "An integrated flexible multifunctional wearable electronic device for personal health monitoring and thermal management," *Sens. Actuators A: Phys.* **318**, 112514 (2021).
- <sup>48</sup>Z. Guo, C. Sun, J. Wang, Z. Cai, and F. Ge, "High-performance laminated fabric with enhanced photothermal conversion and Joule heating effect for personal thermal management," *ACS Appl. Mater. Interfaces* **13**, 8851–8862 (2021).
- <sup>49</sup>P.-C. Hsu, C. Liu, A. Y. Song, Z. Zhang, Y. Peng, J. Xie, K. Liu, C.-L. Wu, P. B. Catrysse, L. Cai, and S. Zhai, "A dual-mode textile for human body radiative heating and cooling," *Sci. Adv.* **3**, e1700895 (2017).
- <sup>50</sup>S. Jafar-Zanjani, M. M. Salary, and H. Mosallaei, "Metafabrics for thermoregulation and energy-harvesting applications," *ACS Photonics* **4**, 915–927 (2017).
- <sup>51</sup>E. M. Leung, M. Colorado Escobar, G. T. Stiubianu, S. R. Jim, A. L. Vyatskikh, Z. Feng, N. Garner, P. Patel, K. L. Naughton, M. Follador, and E. Karshalev, "A dynamic thermoregulatory material inspired by squid skin," *Nat. Commun.* **10**, 1947 (2019).
- <sup>52</sup>S. Assaf, M. Boutghatin, Y. Pennec, V. Thomy, A. Korovin, A. Treizebre, M. Cayette, A. Akjouj, and B. Djafari-Rouhani, "Polymer photonic crystal membrane for thermo-regulating textile," *Sci. Rep.* **10**, 9855 (2020).
- <sup>53</sup>H. Luo, Y. Zhu, Z. Xu, Y. Hong, P. Ghosh, S. Kaur, M. Wu, C. Yang, M. Qiu, and Q. Li, "Outdoor personal thermal management with simultaneous electricity generation," *Nano Lett.* **21**, 3879–3886 (2021).

- <sup>54</sup>B. Xiang, R. Zhang, X. Zeng, Y. Luo, and Z. Luo, “An easy-to-prepare flexible dual-mode fiber membrane for daytime outdoor thermal management,” *Adv. Fiber Mater.* **4**, 1–11 (2022).
- <sup>55</sup>Y. Tao, T. Li, C. Yang, N. Wang, F. Yan, and L. Li, “The influence of fiber cross-section on fabric far-infrared properties,” *Polymers* **10**, 1147 (2018).
- <sup>56</sup>S. G. Johnson and J. D. Joannopoulos, “Block-iterative frequency-domain methods for Maxwell’s equations in a planewave basis,” *Opt. Express* **8**, 173–190 (2001).
- <sup>57</sup>K. Yee, “Numerical solution of initial boundary value problems involving Maxwell’s equations in isotropic media,” *IEEE Trans. Antennas Propag.* **14**, 302–307 (1966).
- <sup>58</sup>A. Taflove, S. C. Hagness, and M. Picket-May, “Computational electromagnetics: The finite-difference time-domain method,” in *The Electrical Engineering Handbook* (Elsevier, 2005), Vol. 3, pp. 629–670.
- <sup>59</sup>A. Taflove, A. Oskooi, and S. G. Johnson, *Advances in FDTD Computational Electrodynamics: Photonics and Nanotechnology* (Artech House, 2013).
- <sup>60</sup>A. F. Oskooi, D. Roundy, M. Ibanescu, P. Bermel, J. Joannopoulos, and S. G. Johnson, “MEEP: A flexible free-software package for electromagnetic simulations by the FDTD method,” *Comput. Phys. Commun.* **181**, 687–702 (2010).
- <sup>61</sup>J.-P. Berenger, “A perfectly matched layer for the absorption of electromagnetic waves,” *J. Comput. Phys.* **114**, 185–200 (1994).